

RNN-based counterfactual prediction, with an application to homestead policy and public schooling

Jason Poulos¹ and Shuxi Zeng²

^{1,2}*Department of Statistical Science, Duke University*

¹*Statistical and Applied Mathematical Sciences Institute (SAMSI)*

Summary

This paper proposes a method for estimating the effect of a policy intervention on an outcome over time. We train recurrent neural networks (RNNs) on the history of control unit outcomes to learn a useful representation for predicting future outcomes. The learned representation of control units is then applied to the treated units for predicting counterfactual outcomes. RNNs are specifically structured to exploit temporal dependencies in panel data, and are able to learn negative and nonlinear interactions between control unit outcomes. We apply the method to the problem of estimating the long-run impact of U.S. homestead policy on public school spending.

Keywords: Counterfactual Prediction; Panel Data; Political Economy; Recurrent Neural Networks; Synthetic Controls

Address for correspondence: Duke University Box 90251, Durham, NC 27708. *E-mail:* jason.poulos@duke.edu. This work was supported by the National Science Foundation Graduate Research Fellowship (DGE 1106400) and used the Extreme Science and Engineering Discovery Environment (XSEDE) Comet GPU at the San Diego Supercomputer Center through allocation SES180010. Code to reproduce the results of the paper is available at <https://github.com/jvpoulos/rnns-causal>.

1 Introduction

An important problem in the social sciences is estimating the effect of a binary treatment on a continuous outcome in a panel data setting. Two prevalent methods for causal inference with panel data are difference-in-differences (DID) and the synthetic control method (SCM). DID uses time-varying panel data to control for time-invariant unobserved confounding, and identifies causal effects by contrasting the change in average outcomes pre- and post-treatment, between treated and control units (e.g., Ashenfelter, 1978). DID assumes no time-varying unobserved confounding that affects both treatment and outcomes, which is highly restrictive and cannot be empirically tested. Moreover, the linear DID estimator assumes i.i.d. errors, which ignores the temporal aspect of the data and understates standard errors for estimated treatment effects when the regression errors are serially correlated, which can arise when the time-series lengths are not sufficiently long to reliably estimate the data generating process (Bertrand et al., 2004).

The SCM is a popular method that constructs a convex combination of control units that are similar to a single treated unit in terms of pretreatment outcomes or covariates (Abadie and Gardeazabal, 2003; Abadie et al., 2010, 2015). The SCM estimator assumes there is a stable convex combination of the control units that absorbs all time-varying unobserved confounding and may be biased even if treatment is only correlated with time-invariant unobserved confounding, which is equivalent to the DID identification assumption (Ferman and Pinto, 2016). The SCM can be generalized to settings in where the time of initial treatment varies across multiple treated units Dube and Zipperer (2015); Ben-Michael et al. (2019) and to include features of DID estimation (Ben-Michael et al., 2018; Arkhangelsky et al., 2019) or Bayesian estimation (Brodersen et al., 2015; Pang et al., 2020).

We propose a method based on recurrent neural networks (RNNs), a class of neural networks that take advantage of the sequential nature of temporal data by sharing model parameters across multiple time periods (El Hihi and Bengio, 1995; Graves, 2012). RNNs have been shown to outperform various linear models on time-series prediction tasks (Cinar

et al., 2017). Unlike the SCM, RNNs are able to learn negative and nonlinear interactions between control unit outcomes, and do not assume a specific activation function when learning representations of the control unit outcomes. RNNs are end-to-end trainable, whereas each component of the Bayesian structural time-series model proposed by Brodersen et al. (2015) must be assembled and estimated independently. RNNs are capable of sharing learned model weights for predicting multiple treated units, and can thus generate more precise predictions in settings where treated units share similar data-generating processes.

We train RNNs on the control units outcomes data to learn a useful latent representation of outcomes in previous periods for predicting future outcomes. We weight the RNNs loss function by the propensity scores modeled in terms of pretreatment covariates to ensure the weighted distribution of the observed confounders are balanced between treated and control units. The learned representation of control unit outcomes is then applied to the outcomes data of the treated units for predicting counterfactual outcomes. The causal effect of treatment on the treated units is estimated by contrasting the counterfactual predictions to the observed outcomes of the treated.

The RNN-based method is related to lagged regression models, which regress post-treatment outcomes on pretreatment outcomes and covariates for control units and then use the model weights to predict the counterfactual outcome for treated units (e.g., Athey et al., 2016; Belloni et al., 2017; Carvalho et al., 2018). A closely related approach are linear factor models, which decompose the pretreatment outcomes of control units into matrices of latent factors (i.e., time-varying coefficients) and factor loadings (i.e., unit-specific intercepts) and predict counterfactual treated unit outcomes based on the estimated factors and loadings (e.g., Xu, 2017; Athey et al., 2017; Amjad et al., 2018). These models typically use regularization or matrix factorization to reduce the dimensionality of the predictor set and thereby improve generalizability when applying the model fit on control units to treated units. These methods all assume unconfoundedness conditional on previous outcomes for control units. The proposed method is also related to doubly-robust estimators that combine

both a propensity score model and an outcome model, which are consistent if either model is properly specified (Bang and Robins, 2005; Chernozhukov et al., 2018). Several studies independent of this work propose using neural networks for counterfactual prediction non-panel observational data settings. For example, Farrell et al. (2018) provide inference results for semiparametric estimation of causal effects using multilayer perceptrons, while Hartford et al. (2017) and Bennett et al. (2019) integrate deep neural networks into an instrumental variables framework.

In the section immediately below, we state the problem of counterfactual prediction within the Neyman-Rubin potential outcomes framework (Neyman, 1923; Rubin, 1990); Section 3 introduces the approach of using RNNs for counterfactual prediction; Section 4 presents the results of placebo tests; Section 5 applies the method to the problem of estimating the long-run impact of U.S. homestead policy on state government investment in public schooling; Section 6 concludes and offers potential avenues for future research.

2 Potential outcomes framework

We explore a panel data setting where we observe a real-valued continuous outcome Y_{it} for each $i = 1, \dots, N$ units and in each $t = 1, \dots, T$ time periods, and where a subset of units is exposed to a binary treatment $W_{it} \in \{0, 1\}$ following an initial treatment period T_0 . We also observe time-invariant pre-treatment covariates, V_{ip} , where p denotes the number of predictors.

We follow the Neyman-Rubin potential outcomes framework (Neyman, 1923; Rubin, 1974, 1990), where there exists a pair of potential outcomes, $Y_{it}(1)$ and $Y_{it}(0)$, corresponding to the response to treatment and control, respectively. The potential outcomes framework implicitly assumes treatment is well-defined to ensure that each unit has the same number of potential outcomes. It also excludes interference between units, which would undermine the framework by creating more than two potential outcomes per unit, depending on the

treatment status of other units. We only observe one of the two potential outcomes for each it value, while the other outcome is counterfactual. The observed outcomes are:

$$Y_{it} = \begin{cases} Y_{it}(0) & \text{if } W_i = 0 \text{ or } t < T_0 \\ Y_{it}(1) & \text{if } W_i = 1 \text{ and } t \geq T_0. \end{cases} \quad (1)$$

Define $\tau_{it} = Y_{it}(1) - Y_{it}(0)$ as the individual treatment effect. The causal estimand of interest is the Average Treatment Effect on the Treated (ATT) at time t and its cumulative version, for time periods $T_0 \leq t \leq T$:

$$\tau_t^{\text{ATT}} = \mathbb{E} [\tau_{it} | W_{it} = 1]; \quad \tau^{\text{ATT}} = \mathbb{E}_t [\tau_t^{\text{ATT}}]. \quad (2)$$

To estimate τ_t^{ATT} , we predict $Y_{it}(0)$ for all it values with $W_{it} = 1$; i.e., the counterfactual outcome of the treated units had they not been exposed to treatment. The counterfactual predictions are subsequently plugged into the estimator:

$$\hat{\tau}_t^{\text{ATT}} = \frac{\sum_{it} W_{it} (Y_{it}(1) - \hat{Y}_{it}(0))}{\sum_{it} W_{it}}. \quad (3)$$

The causal estimand τ_t^{ATT} is identified by assuming that treatment and potential outcomes under control are unconfounded conditional on the pre-treatment outcomes and covariates.

Assumption 1. *Conditional unconfoundedness:*

$$W_{it} \perp\!\!\!\perp Y_{it}(0) \mid Y_{i,1}, \dots, Y_{i,T-1}, V_{ip}.$$

Assumption (1) ensures that treatment assignment affects potential outcomes under control only through covariates and the history of observed outcomes. The idea is that a hypothetical conditional randomization is taking place but, differently from observational studies under the usual strong ignorability assumption (Imbens and Rubin, 2015, Ch. 12), the conditioning

set includes the outcome history.

Assumption 2. *Overlap:*

$$0 < e_{it} < 1.$$

Assumption (2) is needed to summarize the treatment assignment mechanism by propensity score, $e_{it} = \Pr(W_{it} = 1 | Y_{i,1}, \dots, Y_{i,T_0-1}, V_{ip})$. As described in Section 3.1, we use the estimated propensity score to weight the RNNs loss function to correct for imbalances in the distributions of the conditioning set between the treated and control units.

3 RNNs for counterfactual prediction

RNNs operate on n inputs $X = (\mathbf{x}^1, \mathbf{x}^2, \dots, \mathbf{x}^n)^\top = (\mathbf{x}_1, \mathbf{x}_2, \dots, \mathbf{x}_{T_x}) \in \mathbb{R}^{n \times T_x}$, where T_x is the input sequence length. The task is to predict outputs $Y = (\mathbf{y}_1, \mathbf{y}_2, \dots, \mathbf{y}_{T_y}) \in \mathbb{R}^{n \times T_y}$, where output length T_y can differ from T_x , and $T_x + T_y = T$. Given X , we aim to learn a nonlinear mapping $\mathcal{F}(\cdot)$ to predict the next values of the output sequence, $\hat{y}_{t+1} = \mathcal{F}(X)$. RNNs capture nonlinear correlations of the historical values of Y_{it} for $t = 1, \dots, T-1$ to the future values of Y_{it} . The parameter sharing used in RNNs assumes the same learned model parameters is shared for all t ; that is, the estimated nonlinear correlations are stationary.

3.1 Training process

At each t , the RNNs input \mathbf{x}_t and pass it to a fixed-length vector \mathbf{h}_t called the hidden state. \mathbf{h}_t stores information from history of inputs up to \mathbf{x}_t and the previous hidden state, \mathbf{h}_{t-1} . Starting with an initial hidden state \mathbf{h}_0 , \mathbf{h}_t is updated from $t = 1, \dots, T_x$ according to the

forward propagation equations:

$$\mathbf{a}_t = b + Q\mathbf{h}_{t-1} + R\mathbf{x}_t \quad (4)$$

$$\mathbf{h}_t = f(\mathbf{a}_t) \quad (5)$$

$$\hat{\mathbf{y}}_t = d + U\mathbf{h}_t, \quad (6)$$

where Q , R , and U are weight matrices, and b and d are constants. The constants are initialized at zero and \mathbf{h}_0 is initialized by drawing values from a uniform distribution (Glorot and Bengio, 2010). The hidden state activation function in Eq. (5) is a nonlinear function such as the hyperbolic tangent (\tanh), which is a shifted and scaled version of the logistic function that is commonly used with RNNs because the gradient computation is cheaper compared to the logistic function (Socher, 2016).

In Eqs. (4) and (5), the activation function computes the value of \mathbf{h}_t using information from the previous hidden state \mathbf{h}_{t-1} and the current input \mathbf{x}_t . The parameters used to compute \mathbf{h}_t are shared for each value of t . In Eq. (6), the RNNs read information from \mathbf{h}_t to output a sequence of predicted values $\hat{\mathbf{y}}^{(t)}$. The process of forward propagation culminates in producing a loss that compares $\hat{\mathbf{y}}^{(t)}$ and $\mathbf{y}^{(t)}$. Gradients for Eq. (4) and Eq. (7) are computed by the back-propagation through time algorithm (Goodfellow et al., 2016, p. 384), which are subsequently used for gradient descent to estimate the network parameters.

We weight the RNNs objective function to minimize the MSE weighted by the propensity score, which we estimate by multiresponse lasso regression in order to share model parameters across multiple time periods and to shrink the coefficients of (all but one) correlated covariates towards zero (Tibshirani et al., 2012; Simon et al., 2013). In order avoid extreme propensity weights, we employ overlap weighting so that observed values under treatment receive a weight of $1 - \hat{e}_{it}$ and observed values under control receive a weight equal to \hat{e}_{it} (Li

et al., 2018). The propensity-score weighted MSE is:

$$L = \frac{1}{T_y} \sum_{t=1}^{T_y} W_{it} (1 - \hat{e}_{it}) + (1 - W_{it}) \hat{e}_{it} (\hat{\mathbf{y}}_t - \mathbf{y}_t)^2 + \lambda \mathbf{u}_t^2, \quad (7)$$

where the right-hand-side term is the ridge penalty on the learned weights $U = (\mathbf{u}_1, \mathbf{u}_2, \dots, \mathbf{u}_{T_y})$ from Eq. (6) and $\lambda > 0$ controls the regularization strength.

We train RNNs on control outcomes using a sliding window with step size of one. Each sliding window contains $T_0/4$ time periods as input, and aims to predict following time period. Data are fed into the networks in batches of size 32 and the networks are trained for 500 epochs with mini-batch gradient descent on Eq. (7). The last 20% of the training set is reserved for model validation. In order to prevent over-fitting, the training process stops early when there ceases to be improvement on the validation set loss within 25 epochs, and in the event of early stopping, the model weights associated with the lowest validation set loss are restored. In addition to applying a ridge penalty to Eq. (7), we regularize the networks by applying dropout to both the hidden units and recurrent connections (Gal and Ghahramani, 2015).

3.2 Identification

After training, we can impute the missing potential outcomes under control $\widehat{Y}_{it}(0)$ with the forward propagation equations in (4)-(6). We train on the control units to predict the missing outcome $\widehat{Y}_{it}(0)$ for those (i, t) pairs with $W_{it} = 1$. We then estimate τ^{ATT} (3) by contrasting $\widehat{Y}_{it}(0)$ with $Y_{it}(1)$. Under Assumptions (1) and (2), the τ^{ATT} can be identified.

3.3 Network architecture

We employ encoder-decoder networks, which are the standard for neural machine translation (Cho et al., 2014; Bahdanau et al., 2014; Vinyals et al., 2014) and are also widely used for predictive tasks, including speech recognition (e.g., Chorowski et al., 2015) and time-series

forecasting (e.g., Zhu and Laptev, 2017). Encoder-decoder networks consist of an encoder and decoder RNN, both taking the form of long short-term memory (LSTM) networks. LSTMs are designed to resolve problems such as vanishing and exploding gradients that prevent the networks from learning long-term dependencies in the data, which has a tendency to occur when the dimension of the hidden states is too small to summarize long input sequences (Pascanu et al., 2013; Bahdanau et al., 2014).

The encoder RNN reads in X sequentially and the hidden state of the network updates according to Eq. (5). The final hidden state of the encoder is a fixed-size context vector \mathbf{c} that summarizes the input sequence, which is copied over to the decoder RNN. Thus, the hidden state of the decoder is updated recursively by

$$\mathbf{h}_t = f(\mathbf{h}_{t-1}, \mathbf{y}_{t-1}, \mathbf{c}; \theta), \quad (8)$$

and the conditional probability of the next element of the sequence is

$$\Pr(\mathbf{y}_t | \mathbf{y}_1, \dots, \mathbf{y}_{t-1}, \mathbf{c}) = f(\mathbf{h}_{t-1}, \mathbf{y}_{t-1}, \mathbf{c}; \theta). \quad (9)$$

As in Eq. (6), the decoder uses \mathbf{h}_t to predict \mathbf{y}_t at each t .

In our experiments and empirical application, the encoder-decoder networks consist of a two-layer LSTM encoder and single-layer Gated Recurrent Unit (GRU) (Chung et al., 2014) decoder, each with 128 hidden units and tanh activation, stacked on a fully-connected output layer with no activation function, i.e., $f(x) = x$. We compare the encoder-decoder networks with a baseline LSTM consisting of a single-layer LSTM stacked on a fully-connected output layer. The baseline LSTM has fewer network parameters than the encoder-decoder networks, and is expected to be more suitable for smaller-dimensional datasets.

4 Placebo test experiments

We conduct a series of placebo test experiments on data without real interventions in order to evaluate the ability of the RNN-based estimator to recover a null average treatment effect, i.e., $\tau_t^{\text{ATT}} = 0$. The rationale for placebo test experiments is that we know the ground-truth and Assumption (1) is satisfied in expectation because placebo treatment is assigned randomly. For each trial run, we randomly select $N/2$ placebo treated units and predict their outcomes for periods following a given placebo initial time period under a staggered treatment adoption setting.

We benchmark the performance of the encoder-decoder networks and a baseline LSTM against several baseline estimators in terms of the root mean squared error (RMSE), comparing the actual and predicted values. A full description of the benchmark estimators are provided in the Supplementary Material (SM), Section SM-1.

- (a) **DID** Difference-in-differences regression of outcomes on treatment and unit and time fixed effects(Athey and Imbens, 2018);
- (b) **Encoder-decoder** Encoder-decoder network, as described in Section 3.3;
- (c) **LSTM** Baseline single-layer LSTM;
- (d) **MC-NNM** Nuclear norm regularized matrix completion estimator (Athey et al., 2017);
- (e) **SCM** Generalized SCM with the restriction of nonnegative weights and zero intercept of the original SCM, and weights estimated by gradient descent (Doudchenko and Imbens, 2016);
- (f) **SCM-L1** Generalized SCM with an intercept and without weights restrictions, and weights estimated by lasso linear regression (Doudchenko and Imbens, 2016);
- (h) **VAR** Stationary vector autoregression, with weights estimated by lasso linear regression (Kock and Callot, 2015).

The comparison between the RNN-based estimators and the VAR is particularly important because the latter is capable of modeling a linear dependency component, which

is present in most real-world datasets, while the former is suitable for modeling a non-linear dependency component that potentially spans across multiple time periods (Goel et al., 2017). However, RNNs typically require a large amount of training data to effectively capture nonlinear and potentially long-memory dependencies.

To facilitate the comparison, we run placebo test experiments on the dataset underlying our empirical application along with three high-dimensional datasets. The education spending dataset, described in Section 5.1, consists of historical data on per-capita education spending of 49 U.S. state governments over $T = 159$ years. We remove the treated units from the dataset, leaving $N = 18$ control states. The Gaussian process data are smooth signals generated using radial basis function to specify a Gaussian process (GP) with zero-valued mean function. The sine waves data are generated nonlinear variations with frequencies in $[1.0, 5.0]$, amplitudes in $[0.1, 0.9]$, and random phases between $[-\pi, \pi]$. The Gaussian process and sine waves datasets each consist of $N = 4,956$ samples with sequence length of $T = 500$. Lastly, the stock prices dataset consists of stock market returns for $N = 2,453$ stocks over $T = 3,082$ days. The stock market is dynamic, non-stationary and complex in nature, and predicting stock market returns is a challenging task due to its unpredictable and non-linear nature.

In Figure 1, we calculate the autocorrelation function $\rho(k) = \text{Cor}(Y_{t+k}, Y_t)$ for the observations in different placebo test datasets. The correlation decays quickly in the stock prices, sine waves, and gaussian process datasets, which suggests that the outcomes depend mostly on the observations in the short run. On the other hand, the correlation in the education spending data remains prominent for the order lagged before 35, indicating that the dependency along the time dimension is in a longer term and of a more complicated structure. The RNN-based estimators and VAR are expected to hold an advantage over the other estimators in capturing the temporal information or dependency in the long run.

Figure 2 reports average RMSE for each estimator, varying the placebo initial treatment time under randomly assigned treatment in a staggered treatment adoption setting, for the

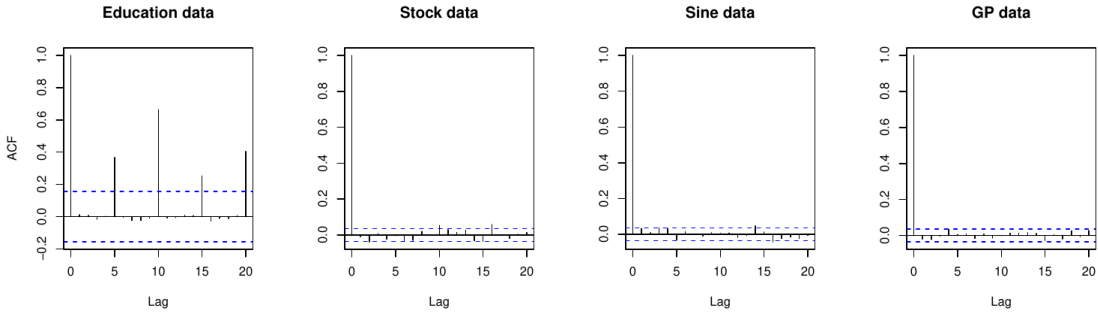


Figure 1: Autocorrelation function for the data in placebo tests. The education spending data shows a higher order lagged correlation than other datasets.

education spending and Gaussian process datasets. The x axis is the ratio of the initial placebo treatment time to the number of periods in the placebo data, so higher values represent more training data, and estimates are jittered across the x axis to avoid overlap. When trained on the education spending data, the average RMSE for the RNN-based estimators decreases as the amount of training data increases, reflecting the need for sufficient time periods. The LSTM and encoder-decoder networks outperform DID, matrix completion, and VAR on the education spending data and perform comparatively to the generalized SCM and lasso SCM when the RNNs have more data to train on; i.e., $T_0/T = 0.75$. When trained on the higher-dimensional Gaussian process data, the baseline LSTM appears to overfit as the training set increases, whereas the encoder-decoder networks yield a average RMSE comparable to the benchmark estimators when $T_0/T = 0.75$.

In Figure 3, we create 10 different sub-samples by selecting the first T daily returns of N randomly selected stocks, keeping the overall data dimension fixed at $NT = 400,000$, focusing on encoder-decoder networks, the generalized SCM, lasso SCM, and VAR. The sub-sampled matrices range from very thin, $N \times T = (200 \times 2,000)$, to very fat, $N \times T = (2,000 \times 200)$. In each case, $N/2$ units are randomly selected for placebo treatment starting at an initial placebo time period of $T/2$. The average RMSE is the highest for the encoder-decoder networks when the data are very thin, which reflects the benefit of training on high-dimensional data. Across the remaining sub-samples, all estimators perform comparatively

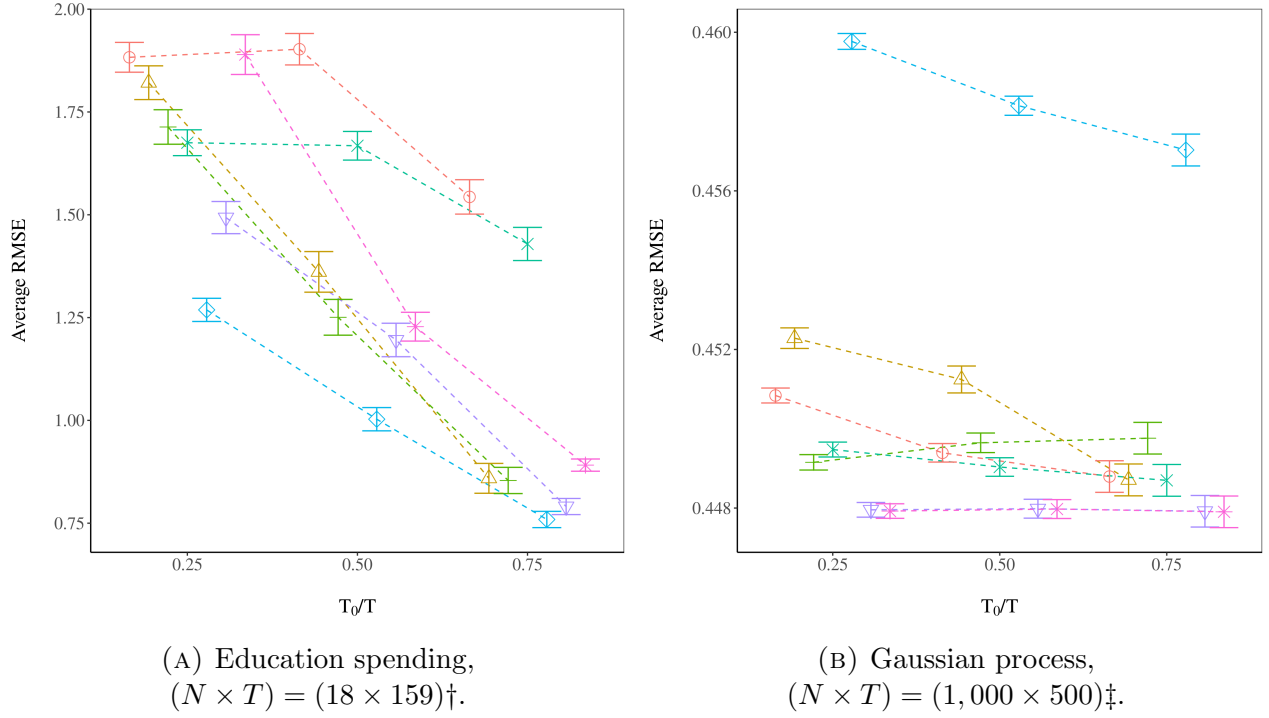


Figure 2: Placebo tests under staggered treatment adoption. Vertical lines represent ± 1.96 times the standard error of the average RMSE across 100 runs. \dagger : Subset from $(N \times T) = (49 \times 159)$; \ddagger : sub-sampled from $(N \times T) = (4,956 \times 500)$. Method: \bigcirc , DID; \triangle , Encoder-decoder (ours); $+$, LSTM (ours); \times , MC-NNM; \diamond , SCM; ∇ , SCM-L1; \ast , VAR.

except for VAR, which is less equipped for handling volatile time-series.

Table 1 reports the average RMSE for the estimators with the placebo initial treatment period set to $T/2$. For the stock prices data, the first $T = 500$ daily returns of $N = 500$ stocks are randomly sub-sampled from the larger dataset. The baseline LSTM outperforms the encoder-decoder networks in the education spending and sine waves datasets, underscoring how the higher complexity of the encoder-decoder networks can hinder performance on datasets with smaller dimensions or those with simple signals, such as with the sine waves data. The VAR is capable of capturing the linear interdependencies among multiple time series and achieves the lowest average RMSE on the Gaussian process dataset, and the generalized SCM and lasso SCM outperform on the other datasets. The matrix completion estimator performs similarly to difference-in-differences, which suggests that the matrix completion estimator relies heavily on unit- and time-fixed effects to make predictions. The RNN-based estimators perform comparatively to the benchmark estimators and outperform both difference-in-differences and matrix completion the education spending and sine waves datasets.

Table 1: Average RMSE on test set under staggered treatment adoption.

	Education spending (18×159) \dagger	Gaussian process ($1,000 \times 500$) \ddagger	Sine waves ($1,000 \times 500$) \ddagger	Stock prices ($1,000 \times 500$) \ddagger
DID	1.902 ± 0.019	0.449 ± 10^{-4}	0.465 ± 0.002	0.023 ± 10^{-4}
Encoder-decoder (ours)	1.361 ± 0.025	0.451 ± 10^{-4}	0.445 ± 0.005	0.023 ± 10^{-4}
LSTM (ours)	1.250 ± 0.022	0.449 ± 10^{-4}	0.392 ± 0.001	0.023 ± 10^{-4}
MC-NNM	1.667 ± 0.017	0.449 ± 10^{-4}	0.455 ± 0.002	0.023 ± 10^{-4}
SCM	1.002 ± 0.014	0.458 ± 10^{-4}	0.347 ± 0.001	0.022 ± 10^{-4}
SCM-L1	1.195 ± 0.020	0.447 ± 10^{-4}	0.284 ± 0.002	0.023 ± 10^{-4}
VAR	1.227 ± 0.017	0.447 ± 10^{-4}	0.387 ± 0.001	0.023 ± 10^{-4}

Notes: Average RMSE \pm 1.96 times the standard error across 100 runs, or 25 runs in the case of the sine waves data, with $N/2$ treated units and $T/2$ treated periods. \dagger : Subset from $(N \times T) = (49 \times 159)$; \ddagger : sub-sampled from $(N \times T) = (4,956 \times 500)$; \ddagger : sub-sampled from $(N \times T) = (2,453 \times 3,082)$.

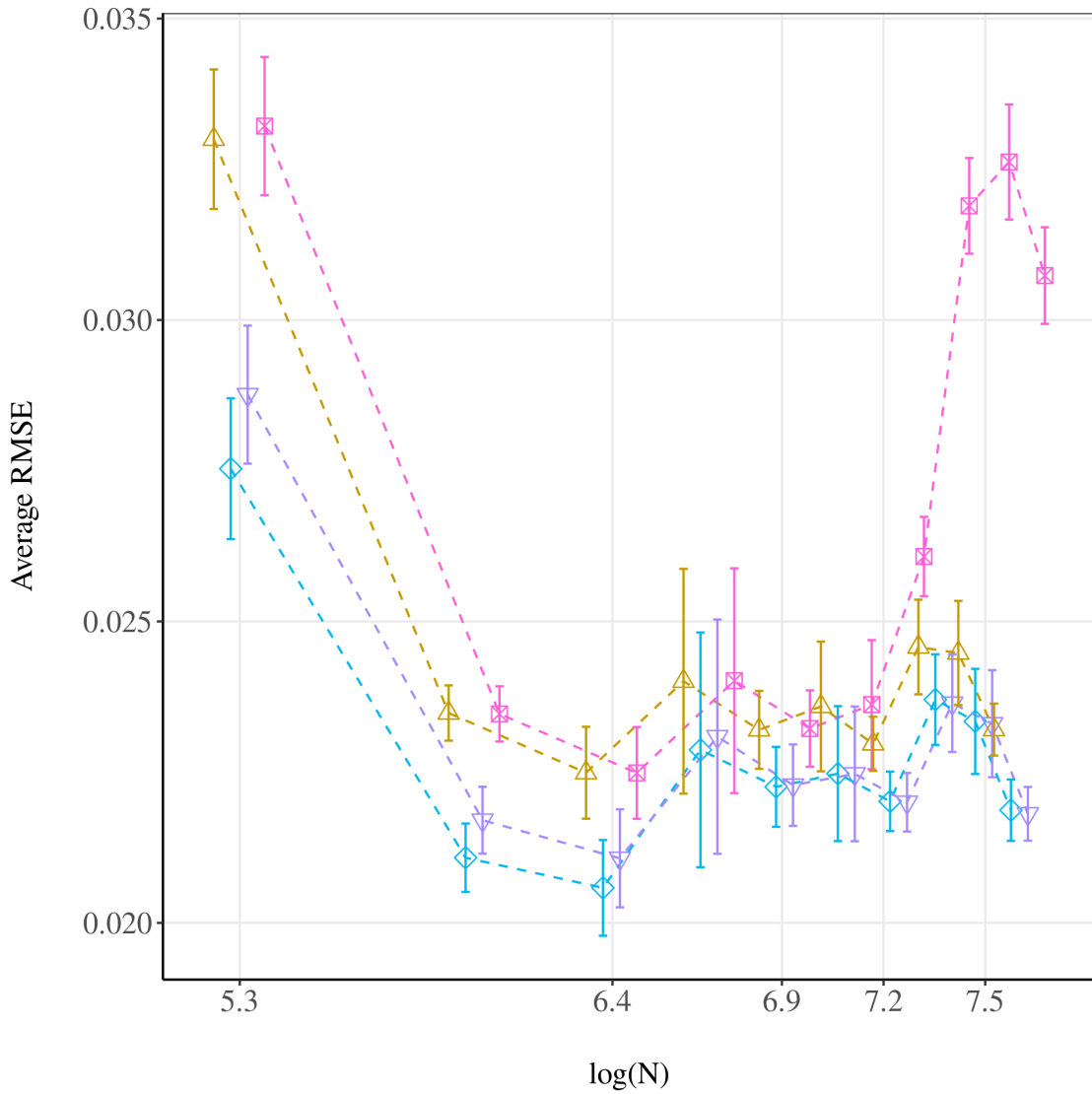


Figure 3: Stock market placebo tests under staggered treatment adoption, with varying dimensions and keeping $N \times T = 400,000$. Vertical lines represent ± 1.96 times the standard error of the average RMSE across 10 runs. Method: \triangle , Encoder-decoder (ours); \diamond , SCM; ∇ , SCM-L1; $*$, VAR.

5 Homestead policy and public schooling in the U.S.

In the empirical application, we are interested in estimating the impact of mid-19th century homestead policy on the development of state government public education spending in the U.S. Social scientists have long viewed the rapid development of public schooling in the U.S. as a nation-building policy (e.g, Meyer et al., 1979; Alesina et al., 2013; Bandiera et al., 2018). According to this view, states across the U.S. adopted compulsory primary education to homogenize the population during the Age of Mass Migration, when tens of millions of foreign migrants arrived to the country between 1850 and 1914.

Engerman and Sokoloff (2005) propose an alternative explanation for the rise of public schooling: state governments on the western frontier expanded investments in public education to attract eastern migrants following the passage of the Homestead Act (HSA) of 1862. The HSA opened for settlement hundreds of millions of acres of frontier land, and any adult citizen could apply for a homestead grant of 160 acres of land, provided that they live and make improvements on the land for five years. According to this view, the sparse population on the frontier meant that state governments competed with each other to attract migrants in order to lower local labor costs and to increase land values and tax revenues. State governments in public land states — i.e., states crafted from the public domain — offered migrants broad access to cheap land and property rights, unrestricted voting rights, and access to public schooling.

Another alternative view is that the HSA led to larger investments in public schooling by reducing the degree of land inequality on the frontier as a consequence of fixing land grants to 160 acres. Political economy frameworks (e.g., Acemoglu and Robinson, 2008; Besley and Persson, 2009) emphasize that greater economic power of the ruling class reduces public investments. In the model of Galor et al. (2009), wealthy landowners block education reforms because public schooling favors industrial labor productivity and decreases the value in farm rents. Inequality in this context can be thought of as a proxy for the amount of *de facto* political influence elites have to block education reforms.

5.1 Data

We draw data on state government education spending from the records of 48 state governments during the period of 1783 to 1932 (Sylla et al., 1993), U.S. Census special reports for the years 1902, 1913, 1932, and 1942, 16 state governments during the period of 1933 to 1937 (Sylla et al., 1995a,b), and U.S. Census special reports for the years 1902, 1913, 1932, and 1942, covering 48 states (Haines, 2010). We inflation-adjust the education spending data according to the U.S. Consumer Price Index and scale by the total free population in the decennial census. We impute missing values in the data by Last Observation Carried Forward (LOCF), which replaces each missing value with the most recent non-missing value prior to it, with remaining missing values carried backward.

Thirty states within the dataset are public land states that were exposed to homesteads authorized by the HSA, while the remaining 19 units are state land states, which were not directly affected by the HSA and therefore serve as control units. The staggered adoption setting is appropriate for this application because T_0 varies across states that were exposed to homesteads following the passage of the HSA. We aggregate approximately 1.46 million records of individual land patents authorized under the HSA to the state level in order to determine how the initial treatment time varies across states (General Land Office). Using these records, we determine that the earliest homestead patents were filed in 1869 in about half of the public land states, while the remaining public land states had patents filed in subsequent years.

To minimize the discrepancy between the covariate distributions of public land states and state land states, we weight the training loss by propensity scores given per-capita education spending during pre-treatment years. We also include in the conditioning set state-level averages of farm sizes and farm values measured in the 1850 and 1860 censuses (Haines, 2010) and the state-level share of total miles of operational railroad track per square mile (Atack, 2013). These pre-treatment covariates control for homesteaders migrating to more productive land and for selection bias arising from differences in access to frontier lands.

While Assumption (1) cannot be directly tested, the placebo tests on pre-treatment data reported in Section 5.4 provide indirect evidence that unconfoundedness is not violated. The no interference assumption also cannot directly be tested; however, it is likely that state land states were indirectly affected by the out-migration of homesteaders from public land states. Interference in this case would likely cause the estimated treatment effect to be understated.

5.2 Main estimates

We train RNNs on the state land states (i.e., control units) and use the learned weights to predict the counterfactual outcomes of public land states (i.e., treated units). The top panel of Figure 4 plots the counterfactual predictions of encoder-decoder networks along with the observed outcomes of treated and control units. Prior to first homestead patent in 1869, the predicted outcomes of the public land states closely track their observed outcomes, which indicates that the networks perform well in the prediction task. The bottom panel plots the differences in the observed and predicted outcomes of the public land states, which are bounded by 95% randomization confidence intervals. We estimate the confidence intervals by constructing a distribution of average placebo effects under the null hypothesis (Cavallo et al., 2013; Hahn and Shi, 2017; Firpo and Possebom, 2018), and describe the estimation procedure in Section SM-2. The confidence intervals include zero for each time period prior to 1869, when no treatment effect is expected.

Counterfactual predictions of state government education spending in the absence of the HSA generally tracks the observed treated outcomes until about 1889, at which the counterfactual flattens and diverges from the increasing observed treated time-series. This delay can potentially be explained by the fact that homesteads did not substantially accumulate until after Congress prohibited the sale of public land in 1889, in all U.S. states except Missouri (Gates, 1941, 1979).

Taking the mean of post-treatment impacts, $\hat{\tau}_t^{\text{ATT}}$, the encoder-decoder estimate of the impact of the HSA on the education spending of public land states is 0.723 log points [0.260,

1.261], as reported in in the first column of Table 2. The confidence intervals surrounding this estimate do not contain zero, which indicates that the estimated effect is significantly more extreme than the exact distribution of average placebo effects under the null hypothesis. To put the magnitude of this point estimate in perspective, it represents about 2.5% of the per-capita total expenditures for public schools in 1929 (Snyder and Dillow, 2010). Table 2 reports the causal estimates recovered by each of the benchmark estimators used in the placebo tests. The LSTM estimated effect is slightly smaller and also statistically significant, 0.547 [0.250, 1.090], whereas the other estimators yield wider confidence intervals that contain zero.

Table 2: ATT estimates by estimator.

	$\hat{\tau}^{\text{ATT}}$	$\hat{\tau}_{\text{placebo}}^{\text{ATT}}$
DID	-1.023 [-3.053, 0.722]	-0.270 [1.668, 1.022]
Encoder-decoder (ours)	0.723 [0.260, 1.261]	-0.021 [-2.160, 1.896]
LSTM (ours)	0.547 [0.250, 1.090]	-0.021 [-2.160, 1.896]
MC-NNM	-0.942 [-2.947, 0.646]	-0.020 [-0.900, 0.738]
SCM	0.397 [-0.402, 1.482]	0.696 [0.266, 2.427]
SCM-L1	0.342 [-0.504, 1.428]	0.536 [-0.373, 1.738]
VAR	0.415 [-0.695, 1.796]	-

Notes: First column is ATT estimates of the impact of the HSA on log per-capita state government education spending. Second column is placebo ATT estimates, with the placebo initial treatment time set to $\frac{2 \times T_0}{3}$. Bracketed values are 95% randomization confidence intervals.

5.3 Sensitivity

We evaluate the sensitivity of the causal estimates to different configurations of RNNs hyperparameters and methods for imputing missing data, reported in Tables SM-1 and SM-2, respectively. We vary the activation used for the hidden layers as tanh or sigmoid (i.e., logistic function); the number of hidden units per hidden layer as 128 or 256; early stopping patience as 50 or 25; and the dropout probability as $p = 0.5$ or $p = 0.2$. The encoder-decoder causal estimates are positive and significant for 12 of the 16 different hyperparameter configura-

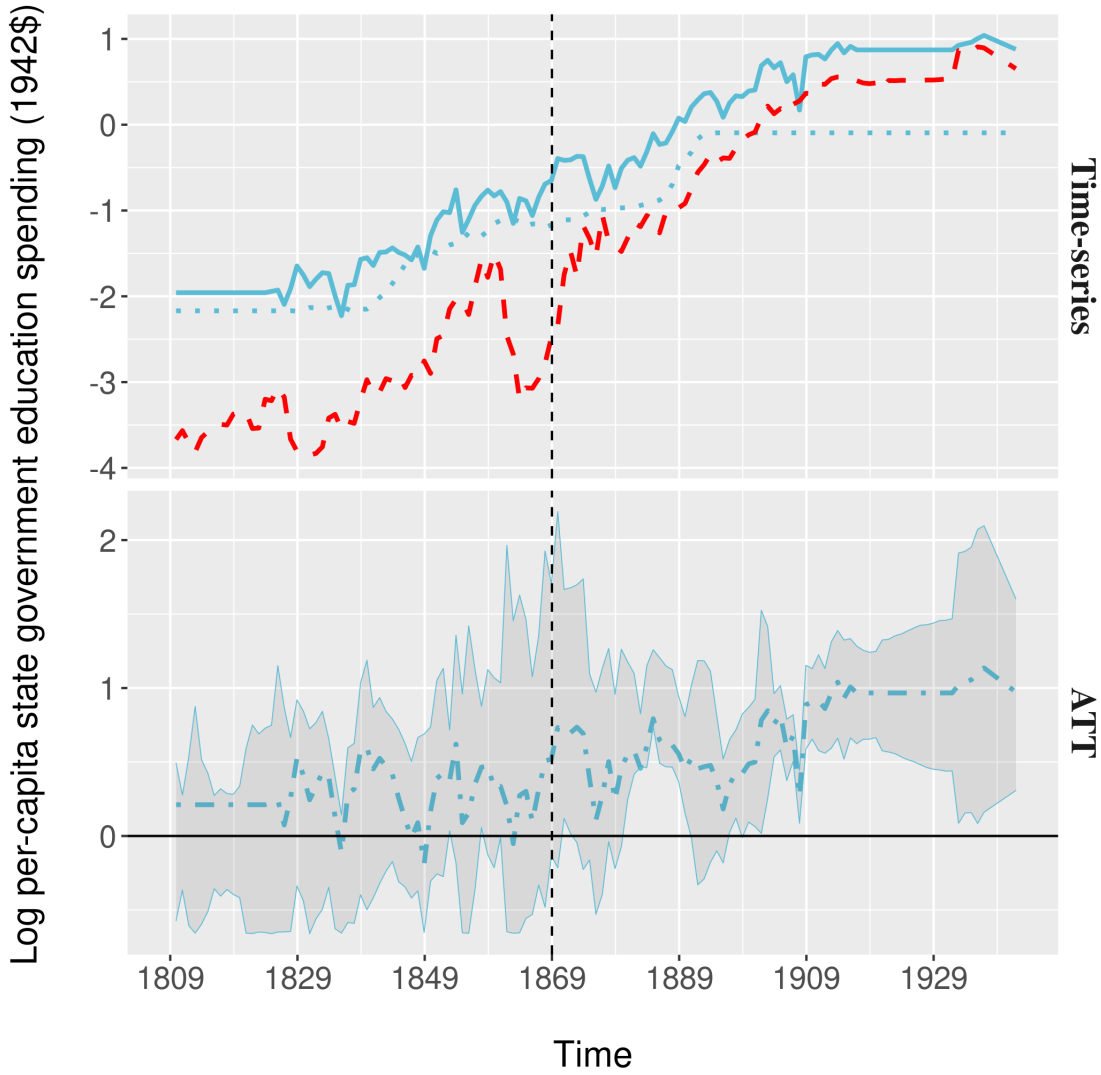


Figure 4: Encoder-decoder estimates of the impact of the HSA on state government education spending, 1809 to 1942, with LOCF imputed missing values. The dashed vertical line represents the first treatment time in 1869. *Key:* —, observed treated; -·-, observed control; ···, counterfactual treated; —·—, $\hat{\tau}_t^{\text{ATT}}$.

tions, while the estimates of the baseline LSTM are more sensitive to different configurations, with only three configurations retaining statistical significance.

In the main analyses, we impute values in the education spending data that are missing due to lack of coverage by LOCF. We run the encoder-decoder networks and benchmark estimators on differently imputed data, using four alternative imputation methods. The encoder-decoder and LSTM causal estimates appear less sensitive to the choice of imputation method compared to the other estimators; however, the confidence intervals for the RNN-based estimators include zero when missing values are randomly replaced or replaced by the mean of the training set.

5.4 Placebo tests

We assess the accuracy of the estimators by conducting placebo tests on the pretreatment data, when no treatment effect is expected. Among the actual treated units, we assign treatment times that are equally spaced between the placebo T_0 , which is two-thirds of the actual T_0 , and $T_0 - 1$. We then construct randomization confidence intervals for the placebo counterfactual trajectories, which we report in the second column of Table 2. For the RNN-based estimators, the confidence intervals contain zero, providing indirect evidence that Assumption (1) is not violated. The other benchmark estimators pass this placebo test, except for the generalized SCM, which estimates a significant causal effect during the pretreatment period. We are unable to recover VAR estimates due to lack of variance in the pretreatment data.

6 Conclusion

This paper makes a methodological contribution in proposing an RNN-based estimator for estimating the effect of a binary treatment in panel data settings. RNNs are specifically structured to exploit temporal dependencies in the data and can learn nonlinear combinations

of control units; the latter is useful when the data-generating process underlying the outcome depends nonlinearly on the history of its inputs. Most real-world time series data have a linear dependency component, for which VARs are suitable, and a nonlinear dependency component that potentially spans across multiple time periods, for which RNNs are suitable. RNNs are unable to handle both linear and nonlinear patterns, which are often both present in real-world time-series, and typically require a large amount of training data to effectively capture nonlinear and potentially long-memory dependencies. In placebo tests, we find that RNN-based estimators perform well in terms of minimizing out-of-sample error compared to VAR and other linear estimators on both small- and high dimensional datasets with varying degrees of temporal dependency. An area of further research is extending the method to combining both linear time-series models such as VAR with RNNs in order to more accurately model complex autocorrelation structures in the data (e.g., Goel et al., 2017).

In the empirical application, we estimate the impact of mid-19th century homestead policy on the development of state government public education spending in the U.S. We train RNNs on states unaffected by homestead policy and use the learned weights to predict the counterfactual outcomes of public land states, which were open to homesteading. The encoder-decoder estimate of the impact of homestead policy on the education spending of public land states is 0.723 log points [0.260, 1.261], which represents about 2.5% of the per-capita total expenditures for public schools in 1929. This estimate is generally robust to the configuration of RNN hyperparameters and the missing data imputation method. The result is consistent with the historical view that state governments in public land states expanded public education investments to attract eastern migrants, or the political economy view that homesteading deterministically lowered land inequality on the frontier and consequently prevented wealthy landowners from blocking public schooling reforms.

References

Abadie, A., Diamond, A. and Hainmueller, J. (2010) Synthetic control methods for comparative case studies: Estimating the effect of California's tobacco control program. *Journal of the American Statistical Association*, **105**, 493–505.

— (2015) Comparative politics and the synthetic control method. *American Journal of Political Science*, **59**, 495–510.

Abadie, A. and Gardeazabal, J. (2003) The economic costs of conflict: A case study of the Basque Country. *The American Economic Review*, **93**, 113–132.

Acemoglu, D. and Robinson, J. A. (2008) Persistence of power, elites, and institutions. *American Economic Review*, **98**, 267–293.

Alesina, A., Giuliano, P. and Reich, B. (2013) Nation-building and education. *Working Paper 18839*, National Bureau of Economic Research. Available at: <http://www.nber.org/papers/w18839>.

Amjad, M., Shah, D. and Shen, D. (2018) Robust synthetic control. *The Journal of Machine Learning Research*, **19**, 802–852.

Arkhangelsky, D., Athey, S., Hirshberg, D. A., Imbens, G. W. and Wager, S. (2019) Synthetic difference in differences. *Tech. rep.*, National Bureau of Economic Research.

Ashenfelter, O. (1978) Estimating the effect of training programs on earnings. *The Review of Economics and Statistics*, 47–57.

Atack, J. (2013) On the use of geographic information systems in economic history: The American transportation revolution revisited. *The Journal of Economic History*, **73**, 313–338.

Athey, S., Bayati, M., Doudchenko, N., Imbens, G. and Khosravi, K. (2017) Matrix Completion Methods for Causal Panel Data Models. *arXiv e-prints*, arXiv:1710.10251.

Athey, S. and Imbens, G. (2018) Design-based analysis in difference-in-differences settings with staggered adoption. *arXiv:1808.05293*.

Athey, S., Imbens, G. W. and Wager, S. (2016) Approximate residual balancing: De-biased inference of average treatment effects in high dimensions.

Bahdanau, D., Cho, K. and Bengio, Y. (2014) Neural Machine Translation by Jointly Learning to Align and Translate. *arXiv e-prints*, arXiv:1409.0473.

Bandiera, O., Mohnen, M., Rasul, I. and Viarengo, M. (2018) Nation-building through compulsory schooling during the age of mass migration. *The Economic Journal*, **129**, 62–109.

Bang, H. and Robins, J. M. (2005) Doubly robust estimation in missing data and causal inference models. *Biometrics*, **61**, 962–973.

Belloni, A., Chernozhukov, V., Fernández-Val, I. and Hansen, C. (2017) Program evaluation and causal inference with high-dimensional data. *Econometrica*, **85**, 233–298.

Ben-Michael, E., Feller, A. and Rothstein, J. (2018) The Augmented Synthetic Control Method. *arXiv e-prints*, arXiv:1811.04170.

Ben-Michael, E., Feller, A. and Rothstein, J. (2019) Synthetic controls and weighted event studies with staggered adoption.

Bennett, A., Kallus, N. and Schnabel, T. (2019) Deep generalized method of moments for instrumental variable analysis. In *Advances in Neural Information Processing Systems 32* (eds. H. Wallach, H. Larochelle, A. Beygelzimer, F. d'Alché-Buc, E. Fox and R. Garnett), 3564–3574. Curran Associates, Inc.

Bertrand, M., Duflo, E. and Mullainathan, S. (2004) How much should we trust differences-in-differences estimates? *The Quarterly Journal of Economics*, **119**, 249–275.

Besley, T. and Persson, T. (2009) The origins of state capacity: Property rights, taxation and politics. *American Economic Review*, **99**, 1218–1244.

Brodersen, K. H., Gallusser, F., Koehler, J., Remy, N. and Scott, S. L. (2015) Inferring causal impact using bayesian structural time-series models. *The Annals of Applied Statistics*, **9**, 247–274.

Carvalho, C., Masini, R. and Medeiros, M. C. (2018) ArCo: An artificial counterfactual approach for high-dimensional panel time-series data. *Journal of Econometrics*, **207**, 352–380.

Cavallo, E., Galiani, S., Noy, I. and Pantano, J. (2013) Catastrophic natural disasters and economic growth. *Review of Economics and Statistics*, **95**, 1549–1561.

Chernozhukov, V., Chetverikov, D., Demirer, M., Duflo, E., Hansen, C., Newey, W. and Robins, J. (2018) Double/debiased machine learning for treatment and structural parameters. *The Econometrics Journal*, **21**, C1–C68. URL: <https://doi.org/10.1111/ectj.12097>.

Cho, K., van Merriënboer, B., Gulcehre, C., Bahdanau, D., Bougares, F., Schwenk, H. and Bengio, Y. (2014) Learning Phrase Representations using RNN Encoder-Decoder for Statistical Machine Translation. *arXiv e-prints*, arXiv:1406.1078.

Chorowski, J. K., Bahdanau, D., Serdyuk, D., Cho, K. and Bengio, Y. (2015) Attention-based models for speech recognition. In *Advances in Neural Information Processing Systems*, 577–585.

Chung, J., Gulcehre, C., Cho, K. and Bengio, Y. (2014) Empirical Evaluation of Gated Recurrent Neural Networks on Sequence Modeling. *arXiv e-prints*, arXiv:1412.3555.

Cinar, Y. G., Mirisaei, H., Goswami, P., Gaussier, E., Aït-Bachir, A. and Strijov, V. (2017) Position-based content attention for time series forecasting with sequence-to-sequence RNNs. In *International Conference on Neural Information Processing*, 533–544. Springer.

Doudchenko, N. and Imbens, G. W. (2016) Balancing, Regression, Difference-In-Differences and Synthetic Control Methods: A Synthesis. *arXiv e-prints*, arXiv:1610.07748.

Dube, A. and Zipperer, B. (2015) Pooling multiple case studies using synthetic controls: An application to minimum wage policies. IZA Discussion Paper No. 8944. Available at: <http://ftp.iza.org/dp8944.pdf>.

El Hihi, S. and Bengio, Y. (1995) Hierarchical recurrent neural networks for long-term dependencies. In *Neural Information Processing Systems*, vol. 400, 409.

Engerman, S. L. and Sokoloff, K. L. (2005) The evolution of suffrage institutions in the new world. *The Journal of Economic History*, **65**, 891–921.

Farrell, M. H., Liang, T. and Misra, S. (2018) Deep neural networks for estimation and inference.

Ferman, B. and Pinto, C. (2016) Revisiting the synthetic control estimator. Available at https://mpra.ub.uni-muenchen.de/81941/1/MPRA_paper_81941.pdf.

Firpo, S. and Possebom, V. (2018) Synthetic control method: Inference, sensitivity analysis and confidence sets. *Journal of Causal Inference*, **6**.

Gal, Y. and Ghahramani, Z. (2015) A theoretically grounded application of dropout in recurrent neural networks.

Galor, O., Moav, O. and Vollrath, D. (2009) Inequality in landownership, the emergence of human-capital promoting institutions, and the great divergence. *The Review of Economic Studies*, **76**, 143–179.

Gates, P. W. (1941) Land policy and tenancy in the prairie states. *The Journal of Economic History*, **1**, 60–82.

— (1979) Federal land policies in the southern public land states. *Agricultural History*, **53**, 206–227.

General Land Office (2017) *General Land Office (GLO) Records Automation*. Bureau of Land Management, Washington, DC.

Glorot, X. and Bengio, Y. (2010) Understanding the difficulty of training deep feedforward neural networks. In *Artificial Intelligence and Statistics*, vol. 9, 249–256.

Goel, H., Melnyk, I. and Banerjee, A. (2017) R2N2: residual recurrent neural networks for multivariate time series forecasting. *CoRR*, **abs/1709.03159**. URL: <http://arxiv.org/abs/1709.03159>.

Goodfellow, I., Bengio, Y. and Courville, A. (2016) *Deep Learning*. Cambridge, MA: MIT press.

Graves, A. (2012) Neural networks. In *Supervised Sequence Labelling with Recurrent Neural Networks*, 15–35. Springer.

Hahn, J. and Shi, R. (2017) Synthetic control and inference. *Econometrics*, **5**, 52.

Haines, M. R. (2010) Historical, Demographic, Economic, and Social Data: The United States, 1790–2002. Ann Arbor, MI: Inter-university Consortium for Political and Social Research [distributor], 2010-05-21. doi.org/10.3886/ICPSR02896.v3.

Hartford, J., Lewis, G., Leyton-Brown, K. and Taddy, M. (2017) Deep IV: A flexible approach for counterfactual prediction. In *Proceedings of the 34th International Conference on Machine Learning* (eds. D. Precup and Y. W. Teh), vol. 70 of *Proceedings of Machine Learning Research*, 1414–1423. International Convention Centre, Sydney, Australia: PMLR. URL: <http://proceedings.mlr.press/v70/hartford17a.html>.

Imbens, G. W. and Rubin, D. B. (2015) *Causal Inference in Statistics, Social, and Biomedical Sciences*. Cambridge: Cambridge University Press.

Kock, A. B. and Callot, L. (2015) Oracle inequalities for high dimensional vector autoregressions. *Journal of Econometrics*, **186**, 325–344.

Li, F., Morgan, K. L. and Zaslavsky, A. M. (2018) Balancing covariates via propensity score weighting. *Journal of the American Statistical Association*, **113**, 390–400.

Meyer, J. W., Tyack, D., Nagel, J. and Gordon, A. (1979) Public education as nation-building in America: Enrollments and bureaucratization in the American states, 1870–1930. *American Journal of Sociology*, **85**, 591–613.

Neyman, J. (1923) On the application of probability theory to agricultural experiments. *Annals of Agricultural Sciences*, **51**. Reprinted in Splawa-Neyman et al. (1990).

Pang, X., Liu, L. and Xu, Y. (2020) A bayesian alternative to synthetic control for comparative case studies. Available at *SSRN*.

Pascanu, R., Mikolov, T. and Bengio, Y. (2013) On the difficulty of training recurrent neural networks. In *International conference on machine learning*, 1310–1318.

Rubin, D. B. (1974) Estimating causal effects of treatments in randomized and nonrandomized studies. *Journal of educational Psychology*, **66**, 688.

— (1990) Comment: Neyman (1923) and causal inference in experiments and observational studies. *Statistical Science*, **5**, 472–480.

Simon, N., Friedman, J. and Hastie, T. (2013) A blockwise descent algorithm for group-penalized multiresponse and multinomial regression.

Snyder, T. D. and Dillow, S. A. (2010) Digest of education statistics, 2009. National Center for Education Statistics. Available at: <https://nces.ed.gov/programs/digest/index.asp>.

Socher, R. (2016) Cs224d deep learning for natural language processing lecture 6: Neural tips and tricks and recurrent neural networks.

Splawa-Neyman, J., Dabrowska, D. M., Speed, T. P. et al. (1990) On the application of probability theory to agricultural experiments. *Statistical Science*, **5**, 465–472.

Sylla, R. E., Legler, J. B. and Wallis, J. (1993) Sources and Uses of Funds in State and Local Governments, 1790–1915: [United States]. Ann Arbor, MI: Inter-university Consortium for Political and Social Research, 2017-05-21. doi.org/10.3886/ICPSR06304.v1.

— (1995a) State and Local Government [United States]: Sources and Uses of Funds, Census Statistics, Twentieth Century [Through 1982]. Ann Arbor, MI: Inter-university Consortium for Political and Social Research, 2017-05-21. doi.org/10.3886/ICPSR06304.v1.

— (1995b) State and Local Government [United States]: Sources and Uses of Funds, State Financial Statistics, 1933–1937. Ann Arbor, MI: Inter-university Consortium for Political and Social Research, 2017-05-21. http://doi.org/10.3886/ICPSR06306.v1.

Tibshirani, R., Bien, J., Friedman, J., Hastie, T., Simon, N., Taylor, J. and Tibshirani, R. J. (2012) Strong rules for discarding predictors in lasso-type problems. *Journal of the Royal Statistical Society: Series B (Statistical Methodology)*, **74**, 245–266.

Vinyals, O., Kaiser, L., Koo, T., Petrov, S., Sutskever, I. and Hinton, G. (2014) Grammar as a Foreign Language. *arXiv e-prints*, arXiv:1412.7449.

Xu, Y. (2017) Generalized synthetic control method: Causal inference with interactive fixed effects models. *Political Analysis*, **25**, 57–76.

Zhu, L. and Laptev, N. (2017) Deep and Confident Prediction for Time Series at Uber. *arXiv e-prints*, arXiv:1709.01907.

Web-Based Supporting Materials for
“RNN-based counterfactual prediction, with an
application to homestead policy and public schooling”
by Jason Poulos and Shuxi Zeng

Table of contents

1	Benchmark estimators	1
1.1	DID	1
1.2	MC-NNM	1
1.3	SCM	1
1.4	SCM-L1	2
1.5	VAR	2
2	Randomization inference	3
3	Tables & Figures	3

1 Benchmark estimators

1.1 DID

The DID model is specified by (Athey and Imbens, 2018):

$$Y_{it} = \gamma_i + \delta_t + \tau W_{it} + \epsilon_{it}, \quad (1)$$

where $\gamma_i + \delta_t$ are unit and time fixed effects, respectively. The model is estimated by least squares:

$$\arg \min_{\tau, \gamma_i, \delta_t} \sum_{i=1}^N \sum_{t=1}^T (Y_{it} - \gamma_i - \delta_t - \tau W_{it})^2. \quad (2)$$

We use the implementation of DID in the `MCPanell` R package, available at <https://github.com/susanathey/MCPanell>.

1.2 MC-NNM

The MC-NNM model is specified by Athey et al. (2017):

$$Y_{it} = L_{it} + \gamma_i + \delta_t + \epsilon_{it}, \quad (3)$$

where L_{it} is a low-rank matrix to be estimated. Estimating L involves minimizing the sum of squared errors via nuclear norm regularized least squares:

$$\arg \min_{L, \gamma, \delta} \left[\frac{1}{|\mathcal{O}|} \sum_{(i,t) \in \mathcal{O}} W_{it} (1 - \hat{e}_{it}) + (1 - W_{it}) \hat{e}_{it} \left(Y_{it} - L_{it} - \gamma_i - \delta_t \right)^2 + \lambda_L \|L\|_{\star} \right], \quad (4)$$

where \mathcal{O} denotes the set of observed (i, t) values. The nuclear norm, or sum of singular values, $\|\cdot\|_{\star} = \sum_i \sigma_i(\cdot)$ is used to yield a low-rank solution for L . In order to place more emphasis on the loss for the values in \mathcal{O} most similar to the missing values in terms of estimated propensity scores, \hat{e}_{it} , we use overlap weights so that observed (i, t) values under treatment receive a weight of $1 - \hat{e}_{it}$ and observed (i, t) values under control receive a weight equal to \hat{e}_{it} . We use the `MCPanell` for implementing MC-NNM under default settings.

1.3 SCM

The synthetic control method (SCM) (Abadie and Gardeazabal, 2003; Abadie et al., 2010, 2015) compares a single treated unit with a synthetic control that combines the outcomes of multiple control units on the basis of their pre-intervention similarity with the treated unit. Doudchenko and Imbens (2016) show that the SCM can be interpreted as regressing the pre-treatment outcomes of a single treated unit on the control unit outcomes during the same periods. The parameters estimated on the controls are used to predict the counterfactual

outcomes for treated unit $i = 0$:

$$\hat{Y}_{0t} = \sum_{i=1}^N \hat{\omega}_i Y_{it}, \quad \forall t = T_0, \dots, T$$

$$\text{where } \hat{\omega} = \arg \min_{\omega} \sum_{s=1}^{T_0} \left(Y_{0s} - \sum_{i=1}^N \omega_i Y_{0s} \right)^2, \quad \text{s.t. } w_i \geq 0, \sum w_i = 1 \quad (5)$$

Eq. (5) imposes the restrictions of the original SCM, namely zero intercept and non-negative regression weights that sum to one. The underlying algorithm for estimating the weights is exponentiated gradient descent (Kivinen and Warmuth, 1997). We use the **MCPanel** R package implementation with default settings, except we clip gradients to the range of $(-5, 5)$.

1.4 SCM-L1

The SCM-EN relaxes the zero-intercept and weight restrictions of Eq. (5). The counterfactual outcomes for treated unit $i = 0$ is:

$$\hat{Y}_{0t} = \hat{\mu} + \sum_{i=1}^N \hat{\omega}_i Y_{it}, \quad \forall t = T_0, \dots, T$$

$$\text{where } (\hat{\mu}, \hat{\omega}) = \arg \min_{\mu, \omega} \sum_{s=1}^{T_0} \left(Y_{0s} - \mu - \sum_{i=1}^N \omega_i Y_{0s} \right)^2. \quad (6)$$

Intuitively, the generalized SCM is a convex combination of control units with intercept μ and weight ω_i for control units i, \dots, N . The model is fit with $N+1$ predictors, including the number of control units and the intercept, and T_0 observations. The estimator is expected to perform better in settings where $T_0 \gg N$ and there are ample observations to fit the model.

Eq. (6) is estimated by lasso regression (Tibshirani, 1996; Tibshirani et al., 2012) in order to reduce the relative size of the predictor set, which is important in cases when $N \gg T_0$. We use the **MCPanel** implementation, of which the underlying algorithm is the **glmnet** package in R (Friedman et al., 2010) with default settings.

1.5 VAR

For a vector of outputs $\mathbf{y}_t = (y_t[1], y_t[2], \dots, y_t[N])^\top$, we fit a stationary vector autoregression with a single lag on the control outcomes:

$$\mathbf{y}_{t+1} = \beta \mathbf{y}_t + \epsilon_{t+1}, \quad \forall y_t[i] \text{ with } W_i = 0. \quad (7)$$

The coefficient matrix β is estimated by lasso regression in order to reduce the size of the predictor set (Callot and Kock, 2014; Kock and Callot, 2015). VAR forecasts on the treated outcomes are made by

$$\hat{\mathbf{y}}_t = \hat{\beta} \mathbf{y}_t, \quad \forall y_t[i] \text{ with } W_i = 1. \quad (8)$$

We use the authors' R package **lassovar** with default settings for implementing VAR, of which the underlying algorithm is the **glmnet** package.

2 Randomization inference

We obtain randomization p -values following these steps:

1. Estimate the actual test static, $\hat{\tau}^{\text{ATT}}$;
2. Calculate every possible average placebo treated effect $\hat{\tau}_{\text{placebo}}^{\text{ATT}}$ by randomly sampling without replacement which $J - 1$ control units are assumed to be treated. There are

$$Q = \sum_{g=1}^{J-1} \binom{J}{g}$$

possible average placebo effects. Since calculating Q can be computationally burdensome for relatively high values of J , we set $Q = 10,000$. The result is a matrix of dimension $Q \times T$;

3. Sum over the time dimension the number of $\hat{\tau}_{\text{placebo}}^{\text{ATT}}$ that are greater than or equal to $\hat{\tau}^{\text{ATT}}$.

Each element of the vector obtained from Step 3 is divided by Q to estimate a T -length vector of exact two-sided p values, \hat{p} .

Under the assumption that treatment has a constant additive effect Δ , we construct an interval estimate for Δ by inverting the randomization test. Let δ_Δ be the test statistic calculated by subtracting all possible μ by Δ . We derive a two-sided randomization confidence interval by collecting all values of δ_Δ that yield \hat{p} values greater than or equal to significance level $\alpha = 0.05$. We find the endpoints of the confidence interval by randomly sampling 500 values of Δ .

3 Tables & Figures

Table 1: ATT estimates by RNNs hyperparameter configuration.

				Encoder-decoder	LSTM
<i>Hidden activation</i>	<i>Hidden units</i>	<i>Patience (epochs)</i>	<i>Dropout (p)</i>		
sigmoid	256	50	0.5	1.005 [0.166, 2.199]	0.607 [-0.301, 1.761]
tanh	256	50	0.5	0.845 [0.315, 2.010]	0.769 [0.224, 1.905]
sigmoid	128	50	0.5	1.154 [0.373, 2.377]	0.628 [-0.266, 1.815]
tanh	128	50	0.5	0.817 [0.305, 1.943]	0.804 [0.259, 1.963]
sigmoid	256	25	0.5	0.541 [-0.375, 1.691]	0.559 [-0.409, 1.715]
tanh	256	25	0.5	0.791 [0.295, 1.922]	0.619 [-0.225, 1.705]
sigmoid	128	25	0.5	0.655 [-0.291, 1.811]	0.647 [-0.227, 1.844]
tanh	128	25	0.5	0.744 [0.218, 1.824]	0.731 [0.229, 1.902]
sigmoid	256	50	0.2	1.063 [0.252, 2.279]	0.540 [-0.441, 1.744]
tanh	256	50	0.2	0.828 [0.336, 2.071]	0.667 [-0.003, 1.760]
sigmoid	128	50	0.2	1.096 [0.208, 2.304]	0.512 [-0.521, 1.704]
tanh	128	50	0.2	0.855 [0.346, 2.098]	0.655 [-0.010, 1.778]
sigmoid	256	25	0.2	0.728 [-0.132, 1.915]	0.485 [-0.548, 1.658]
tanh	256	25	0.2	0.855 [0.315, 2.110]	0.610 [-0.130, 1.836]
sigmoid	128	25	0.2	0.629 [-0.332, 1.824]	0.541 [-0.451, 1.767]
tanh	128	25	0.2	0.794 [0.314, 2.016]	0.640 [-0.141, 1.768]

Notes: estimates of the impact of the HSA on log per-capita state government education spending (1942\\$). Bracketed values are 95% randomization confidence intervals for $\hat{\tau}^{\text{ATT}}$. The highlighted row indicates the RNNs hyperparameter configuration used for the RNN-based estimators in the placebo test experiments on the **education** dataset and in the application.

Table 2: ATT estimates by estimator and imputation method.

<i>Imputation method:</i>	Linear interpolation	Mean replacement	Moving avg. replacement	Random replacement
DID	-0.992 [-2.928, 0.723]	-0.581 [-1.843, 0.611]	-1.076 [-3.039, 0.579]	-0.545 [-2.036, 0.841]
Encoder-decoder (ours)	0.793 [0.307, 1.278]	0.539 [-0.096, 1.170]	0.804 [0.351, 1.328]	0.514 [-0.518, 1.617]
LSTM (ours)	0.730 [0.265, 1.203]	0.448 [-0.148, 1.033]	0.731 [0.268, 1.221]	0.568 [-0.251, 1.380]
MC-NNM	-0.856 [-2.729, 0.490]	-0.243 [-1.309, 0.243]	-0.930 [-2.824, 0.479]	-0.396 [-1.790, 0.847]
SCM	0.465 [-0.299, 1.446]	0.272 [-0.480, 1.166]	0.493 [-0.151, 1.443]	0.217 [-0.557, 1.170]
SCM-L1	0.344 [-0.520, 1.323]	0.203 [-0.572, 1.001]	0.473 [-0.473, 1.482]	0.537 [-0.399, 1.785]
VAR	0.676 [-0.394, 2.041]	0.673 [-0.127, 2.008]	0.599 [-0.476, 1.944]	0.792 [0.138, 2.220]

Notes: ATT estimates with differently imputed missing values. Bracketed values are 95% randomization confidence intervals for $\hat{\tau}^{\text{ATT}}$. Linear interpolation uses linear interpolation to replace missing values; mean replacement replaces missing values with the mean of the training set; moving average replacement replaces missing values with the exponential weighted moving average of the training set; random replacement replaces each missing value by drawing a random sample between the minimum and the maximum non-missing values in the data.

References

Abadie, A., Diamond, A. and Hainmueller, J. (2010) Synthetic control methods for comparative case studies: Estimating the effect of California’s tobacco control program. *Journal of the American Statistical Association*, **105**, 493–505.

— (2015) Comparative politics and the synthetic control method. *American Journal of Political Science*, **59**, 495–510.

Abadie, A. and Gardeazabal, J. (2003) The economic costs of conflict: A case study of the Basque Country. *The American Economic Review*, **93**, 113–132.

Athey, S., Bayati, M., Doudchenko, N., Imbens, G. and Khosravi, K. (2017) Matrix Completion Methods for Causal Panel Data Models. *arXiv e-prints*, arXiv:1710.10251.

Athey, S. and Imbens, G. (2018) Design-based analysis in difference-in-differences settings with staggered adoption. *arXiv:1808.05293*.

Callot, L. A. and Kock, A. B. (2014) Oracle efficient estimation and forecasting with the adaptive lasso and the adaptive group lasso in vector autoregressions. *Essays in Nonlinear Time Series Econometrics*, 238–268.

Doudchenko, N. and Imbens, G. W. (2016) Balancing, Regression, Difference-In-Differences and Synthetic Control Methods: A Synthesis. *arXiv e-prints*, arXiv:1610.07748.

Friedman, J., Hastie, T. and Tibshirani, R. (2010) Regularization paths for generalized linear models via coordinate descent. *Journal of Statistical Software*, **33**, 1.

Kivinen, J. and Warmuth, M. K. (1997) Exponentiated gradient versus gradient descent for linear predictors. *Information and Computation*, **132**, 1–63.

Kock, A. B. and Callot, L. (2015) Oracle inequalities for high dimensional vector autoregressions. *Journal of Econometrics*, **186**, 325–344.

Tibshirani, R. (1996) Regression shrinkage and selection via the lasso. *Journal of the Royal Statistical Society. Series B (Methodological)*, 267–288.

Tibshirani, R., Bien, J., Friedman, J., Hastie, T., Simon, N., Taylor, J. and Tibshirani, R. J. (2012) Strong rules for discarding predictors in lasso-type problems. *Journal of the Royal Statistical Society: Series B (Statistical Methodology)*, **74**, 245–266.